Commun. Comput. Phys.
doi: 10.4208/cicp.2009.09.096

Vol. 7, No. 4, pp. 779-792
April 2010

The Study of the Three-Dimensional Spin-3/2 Ising Model on a Cellular Automaton

N. Seferoğlu*

Advanced Technologies Department, Institute of Science and Technology, Gazi University, Ankara, Turkey.

Received 5 June 2009; Accepted (in revised version) 28 July 2009

Communicated by Dietrich Stauffer

Available online 3 November 2009

Abstract. The spin-3/2 Ising model on the simple cubic lattice with nearest-neighbour ferromagnetic bilinear interaction ($J>0$) is simulated on a cellular automaton by using the cooling algorithm improved from the Creutz cellular automaton. The phase diagrams of the model are constructed in the (D/J, kT/J) and (K/J, kT/J) plane. Comparison of the results are made with those of other methods. The temperature dependence of the order parameters and associated fluctuations are calculated at various of the model parameters and the static critical exponents are estimated within the framework of the finite-size scaling. The results are compatible with the universal Ising critical behavior except for $D/J=-3$ and $K/J=-2.3$.

PACS: 64.60.Cn, 64.60.Fr

Key words: Spin-3/2 Ising model, Creutz cellular automaton, phase diagram, critical exponents, simple cubic lattice.

1 Introduction

The Hamiltonian of the spin-3/2 Ising model with bilinear (J) and biquadratic (K) interactions and a single-spin anisotropy parameter (D), also known as the spin-3/2 Blume-Emery-Griffiths (BEG) model, is

$$H_I=-J\sum_{<ij>}S_iS_j-K\sum_{<ij>}S_i^2S_j^2+D\sum_i S_i^2, \tag{1.1}$$

where the spin variables S_i located at site i on a discrete lattice can take the values $\pm 3/2$, $\pm 1/2$ and the first two summations run over all nearest-neighboring pairs.

*Corresponding author. *Email address:* nurguls@gazi.edu.tr (N. Seferoğlu)

In recent years, much attention has been directed to the spin-3/2 Ising systems [1] which was initially introduced to give a qualitative description of phase transition observed in the compound DyVO4 and also to study tricritical properties in ternary mixtures [2].

There has been a number of theoretical studies to obtain the phase diagrams and critical and multicritical behavior of the model. All these studies were done by different methods, such as mean field approximation (MFA) [1–4], renormalization group (RG) methods [5,6], the effective-field theory (EFT) [7–9], cluster variation method (CVM) [10–12] and Monte Carlo (MC) simulation [3,13]. Most of these studies have considered some portion of the phase diagram of the model. Within the MFA and MC calculations [3], only the phase diagrams of the isotropic spin-3/2 BEG model and the spin-3/2 BC model which includes only J and K interactions were obtained. These models were also studied by using the EFT [8] and CVM [10]. Recently, the phase diagrams of the spin-3/2 BEG model in the (D/J, kT/J) plane for several values of K/J and in the (K/J, kT/J) plane for several values of D/J have been presented [6,11,12]. In spite of these studies, further studies using alternative methods are desirable to obtain the new phase diagrams and the critical behavior of the model. However, as far as we know, there is no extensive analysis within the framework of the finite-size scaling theory to determine the static critical exponents of the spin-3/2 BEG model in three dimensions.

In this paper, the critical behavior of the three-dimensional spin-3/2 BEG model has been studied by using an improved algorithm from the Creutz Cellular Automaton (CCA). Our interest is focused to obtain the phase diagrams in the (D/J, kT/J) and (K/J, kT/J) planes and estimate the static critical exponents on three dimensional lattice within the framework of finite-size scaling theory. The CCA algorithm is a microcanonical algorithm interpolating between the canonical Monte Carlo and molecular dynamics techniques on a cellular automaton, and it was first introduced by Creutz [14]. In the previous papers [14–21], the CCA algorithm and improved algorithms from CCA were used to study the critical behavior of the different Ising model Hamiltonians in two and three dimensions. It was shown that they have successfully produced the critical behavior of the models. The remainder of this paper is organized as follows: The details of the model are explained in Section 2, the results are discussed in Section 3 and a conclusion is given in Section 4.

2 Model

Three variables are associated with each site of the lattice. The value of each sites is determined from its value and those of its nearest-neighbors at the previous time step. The updating rule, which defines a cellular automaton, is as follows: Of the three variables on each site, the first one is Ising spin S_i. The Ising spin energy for the model is given by Eq. (1.1). The second variable is for momentum variable conjugate to the spin (the demon). The kinetic energy associated with the demon is $H_k = nJ$, where n is an integer,

which can take a value within the interval (0, m). The total energy

$$H = H_I + H_K \tag{2.1}$$

is conserved.

The third variable provides a checkerboard style updating, and so it allows the simulation of the Ising model on a cellular automaton. The black sites of the checkerboard are updated and then their color is changed into white; white sites are changed into black without being updated. The updating rules for the spin and the momentum variables are as follows: For a site to be updated its spin is changed into one of the other three states with equal probability and the change in the Ising energy, dH_I, is calculated. If this energy is transferable to or from the momentum variable associated with this site, such that the total energy H is conserved, then this change is done and the momentum is appropriately changed. Otherwise the spin and the momentum are not changed.

For a given total energy the system temperature is obtained from the average value of kinetic energy, which is given by:

$$< E >= \frac{\sum_{n=0}^{m} Jne^{-nJ/kT}}{\sum_{n=0}^{m} e^{-nJ/kT}}, \tag{2.2}$$

where $E = H_K$. The expectation value in Eq. (2.2) is a average over the lattice and the number of the time steps. Because of the third variable, the algorithm requires two time steps to give every spin of the lattice a chance to change. Thus, in comparison to ordinary Monte Carlo simulations, two steps correspond to one full sweep over the system variables.

The cooling algorithm is divided into two basic parts, initialization procedure and the taking of measurements. In the initialization procedure, firstly, all spins in the lattice sites take the ferromagnetic ordered structure and staggered quadrupole ordered structure according to selected (J,K,D) parameter set and the kinetic energy per site which is equal to the maximum change in the Ising spin energy for the any spin flip is given to the lattice sites via the second variables. This configuration is run during 10.000 cellular automaton time steps. At the end of the this step, the configuration in the disordered structure at the high temperature is obtained. In the next steps, the last configuration in the disordered structure has been chosen as a starting configuration for the cooling run. Rather than resetting the starting configuration at each energy, it is used the final configuration at a given energy as the starting point for the next. During the cooling cycle, energy is subtracted from the system through the second variables (H_k) after 1.000.000 cellular automaton steps.

3 Results and discussion

3.1 Phase diagrams

The simulations are carried on $L\times L\times L$ simple cubic lattice with $L=12$, 14, 16, 18, 24 and 30. The periodic boundary conditions are applied in all directions. The computed values of the quantities are averages over the lattice and over the number of time steps (1.000.000) with discard of the first 100.000 time steps during which the cellular automaton develops.

The physical quantities computed in our simulations are the sublattice order parameters (M_α and Q_α, $\alpha=A$ or B) and the order parameter Q_d:

$$M_\alpha=\frac{2}{N}\sum_\alpha S_i^\alpha, \tag{3.1}$$

$$Q_\alpha=\frac{2}{N}\sum_\alpha (S_i^\alpha)^2, \tag{3.2}$$

$$Q_d=\frac{2}{N}\left(\sum_A (S_i^A)^2-\sum_B (S_i^B)^2\right), \tag{3.3}$$

and the susceptibilities associated to the M_α and Q_d

$$\chi_\alpha=\beta N<M_\alpha^2>-<M_\alpha>^2, \tag{3.4}$$

$$\chi_d=\beta N<Q_d^2>-<Q_d>^2, \tag{3.5}$$

where N is the total number of sites of the lattice.

For $J>0$, the possible phases of the model are defined according to the values of the two sublattice order parameters:

disordered phase (d):	$M_A=M_B=0$,	$Q_A=Q_B\neq 0$;
ferromagnetic phase (f):	$M_A=M_B\neq 0$,	$Q_A=Q_B$;
ferrimagnetic phase (fr):	$M_A\neq M_B\neq 0$,	$Q_A\neq Q_B\neq 0$;
antiquadrupolar phase (a):	$M_A=M_B=0$,	$Q_A\neq Q_B\neq 0$.

In this study, four phase diagrams are obtained for selected K/J and D/J values. To produce the phase diagrams, the finite critical temperatures are estimated from the maxima of the fluctuations of the order parameters on the lattice with $L=16$. In Fig. 1, the phase diagram obtained for $D/J=0$ in the (K/J, kT/J) plane is given. In this figure, the CVM [10] and MC [3] results are shown to compare with our results. It is seen that the phase diagram contains d and f phases and also fr phase which occurs at low temperature inside the f region. All the boundaries among these phases are all second-order lines. However, there is only a transition from the d phase to the f phase at the d-f phase boundary. At low temperature, $f\rightarrow fr$ and $f\rightarrow fr\rightarrow f$ transitions occur at the f-fr phase

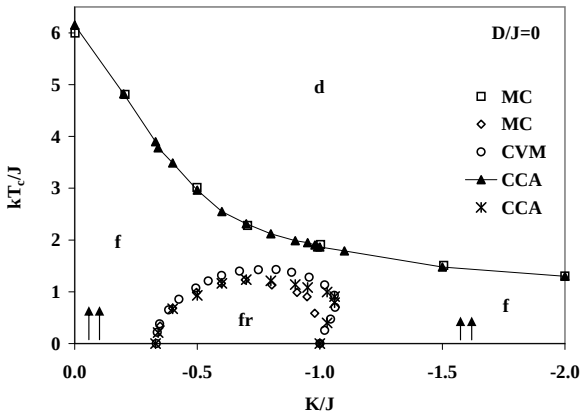

Figure 1: The phase diagram in the $(K/J,\ kT/J)$ plane for $D/J=0$.

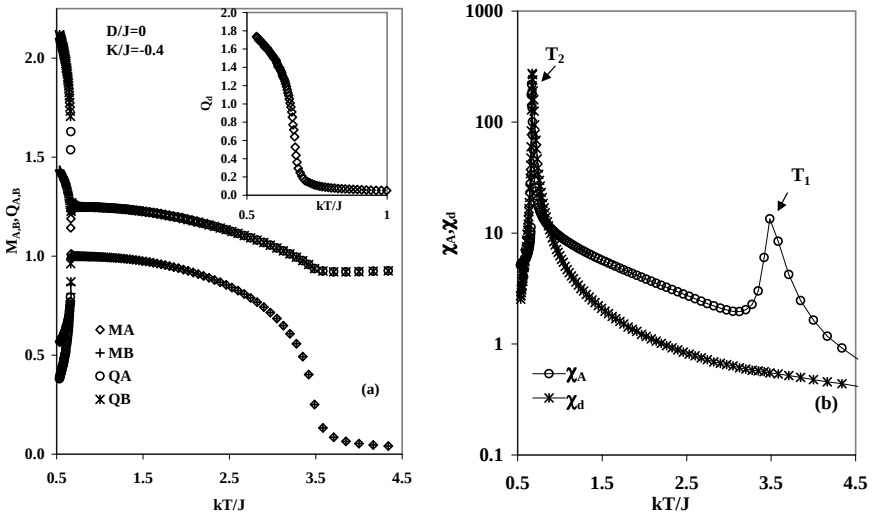

Figure 2: The temperature dependence of a) the sublattice order parameters M_A, M_B, Q_A and Q_B and the order parameter Q_d (inset in figure), b) the susceptibilities χ_A and χ_d at $D/J=0$ for $K/J=-0.4$ on a lattice with $L=16$.

boundary. This line also exhibits re-entrant behavior as the MFA [3], CVM [10, 12] predictions, but differs from the MC [3] and EFT [8] results which predicted no re-entrant behavior.

In Fig. 2, the temperature dependence of the order parameters and susceptibilities are shown for $K/J=-0.4$ where the $d\to f\to fr$ phase transition occurs. As it is seen in the Fig. 2, the sublattice order parameters are equal at high temperature and $d\to f$ transition occurs as the temperature decreases. The $f\to fr$ transition occurs at low temperature and the sublattice order parameters become unequal as the temperature is lowered and tend to be M_A=0.5 and M_B=1.5 at zero temperature. However, Q_d order parameter seen in the

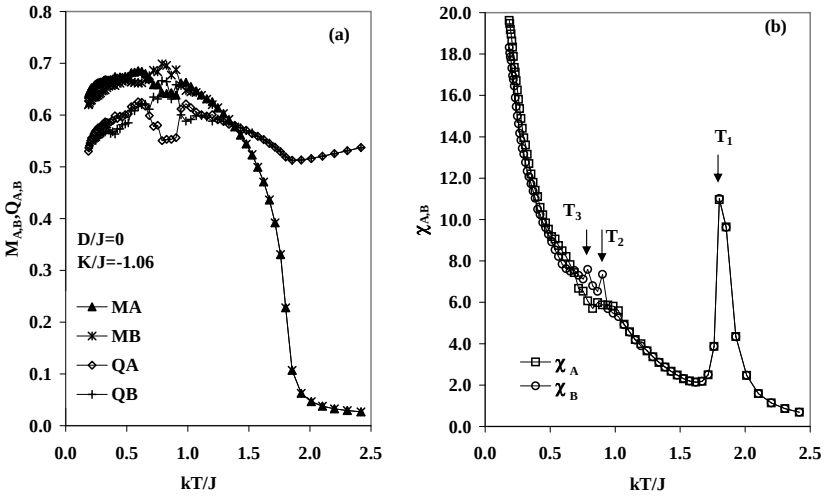

Figure 3: The temperature dependence of a) the sublattice order parameters M_A, M_B, Q_A and Q_B, b) the susceptibilities χ_A and χ_B at $D/J=0$ for $K/J=-1.06$ on a lattice with $L=16$.

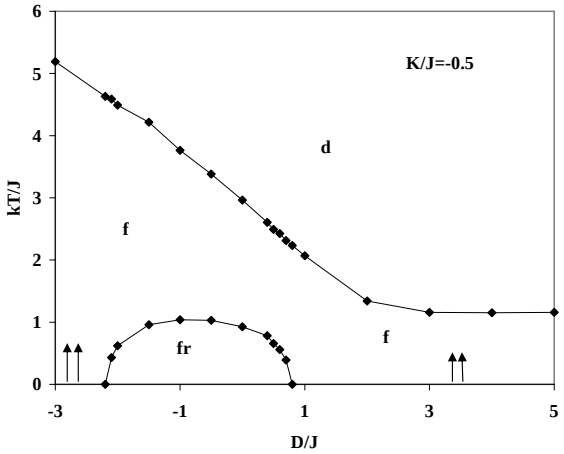

Figure 4: The phase diagram obtained in the $(D/J,\ kT/J)$ plane for $K/J=-0.5$.

inset Fig. 2(a) exhibits a continuous behavior which characterizes the $f \to fr$ transition. The data of the sublattice susceptibilities show the two peaks which belong the $d \to f$ and $f \to fr$ transitions. However, the susceptibility χ_d has a peak for $f \to fr$ transition and no singularity belongs to the $d \to f$ as expected (Fig. 2(b)). On the other hand, the re-entrant behavior occurs in a small range of K/J. An example of the $d \to f \to fr \to f$ transitions is shown for $K/J=-1.06$ in Fig. 3. The sublattice order parameters undergo three successive transitions and these transitions are second order (Fig. 3(a)). At the same time, the sublattice susceptibilities show three peaks at T_1, T_2 and T_3 for $d \to f$ and $f \to fr$ and $fr \to f$, respectively (Fig. 3(b)). However, it is obtained that the Q_d order parameter is not useful to detect a transition in the re-entrant region.

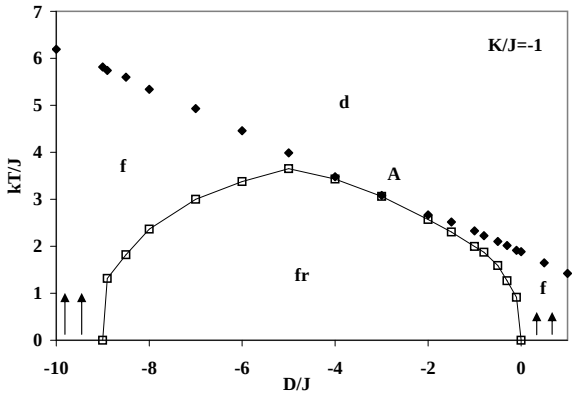

Figure 5: The phase diagram obtained in the $(D/J,\ kT/J)$ plane for $K/J=-1$.

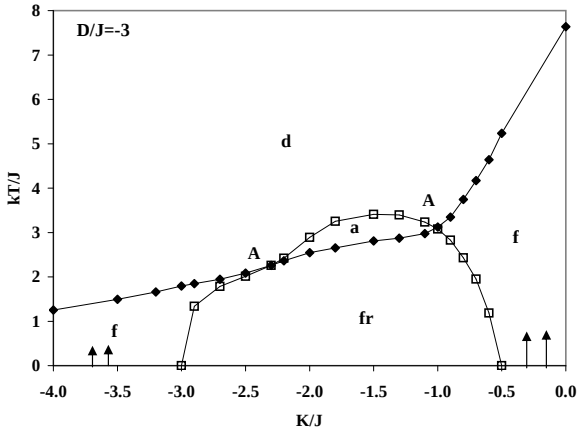

Figure 6: The phase diagram obtained in the $(K/J,\ kT/J)$ plane for $D/J=-3$.

In Fig. 4, the phase diagram obtained for $K/J=-0.5$ is shown. The phase diagram contains a second-order line between the d and f phases and the other line between the f and fr phases. The fr phase occurs in the range of $-2.2<D/J<0.8$. The topology of this phase diagram is very similar to the phase diagram for $D/J=0$ except the occurrence of reentrancy at the f-fr phase boundary. It should be mentioned that although the similar topology was presented for various parameters in the literature [12], the phase diagram for $K/J=-0.5$ has not been obtained by previous calculations.

The other phase diagram obtained in the $(D/J,\ kT/J)$ plane for $K/J=-1$ is shown in Fig. 5. As seen in figure, the fr phase lies in the region $-9<D/J<0$ within the ferromagnetic phases at low temperatures. However, the phase diagram exhibits one multicritical point (A). Similar phase diagram was also obtained by the CVM [12] for $K/J=-1$ but differs from in that the reentrant behavior was found in this work.

Before concluding this section, we present the phase diagram obtained for $D/J=-3$ (Fig. 6). As far as we know, this phase diagram has gone unnoticed in the other

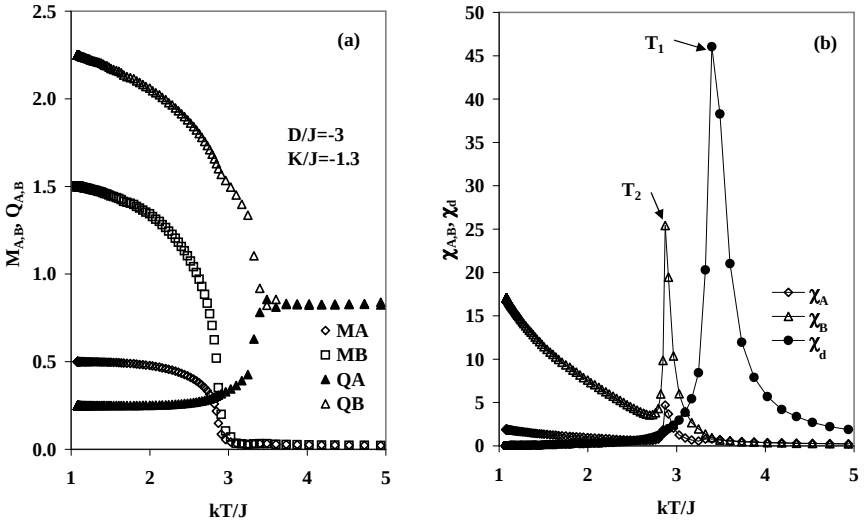

Figure 7: The temperature dependence of a) the sublattice order parameters M_A, M_B, Q_A and Q_B, b) the susceptibilities χ_A, χ_B and χ_d at $D/J=-3$ for $K/J=-1.3$ on a lattice with $L=16$.

approximations. According to our calculations, there is only $d \to f$ transition for $K/J < -3$ and $K/J > -0.5$. The $d \to f \to fr$ transitions take place in the interval $-3 < K/J < -2.3$ and $-1 < K/J < -0.5$. The phase diagram also contains the a phase which lies between the d and fr phase and the $d \to a \to fr$ transitions occur in the interval $-2.3 \leq K/J < -1$. However, the phase diagram also exhibits the two multicritical points (A), as seen in figure. In Fig. 7, the sublattice order parameters are presented for the $d \to a \to fr$ transition at $K/J = -1.3$ value. For the transition from the d phase to the a phase, the values of M_A and M_B remain at zero value and Q_A and Q_B become unequal with decreasing temperature. Therefore, the sublattice susceptibilities have no information about this transition, only one peak belongs to the lower $a \to fr$ transition. On the other hand, the order parameter Q_d shows the nature of the transition $d \to a$ and the χ_d has a peak belongs to $d \to a$ transition (Fig. 7(b)). Therefore, in this diagram, the d-a phase boundary was produced from the maxima of the susceptibility χ_d.

3.2 FSS analysis

The static critical exponents are estimated by using the finite-size scaling (FSS) analysis for selected D/J and K/J values. In the following, a detailed of these analysis is given:

The critical temperature values for the finite-size scaling analysis are estimated from the temperature variation of the Binder fourth-order cumulant [22, 23] of the order parameters M_α and Q_d ($g_L^{M_\alpha}$ and $g_L^{Q_d}$).

The critical exponents ν can be obtained by using the finite-size scaling relation for

the Binder cumulant, which is defined by [23]:

$$g_L = G(\varepsilon L^{1/\nu}), \tag{3.6}$$

where $\varepsilon=(T-Tc(\infty))/Tc(\infty)$. It is explained in previous section that the order parameter Q_d is useful for detecting the $f\to fr$ and $d\to a$ transitions. On this account, the infinite lattice critical temperatures $T_c^{g_L^{M_\alpha}}(\infty)$ and $T_c^{g_L^{Q_d}}(\infty)$ are obtained from the intersection of the $g_L^{M_\alpha}$ and $g_L^{Q_d}$ curves for different lattice sizes for the related transitions. In Fig. 8(a), the temperature variations of the $g_L^{Q_d}$ belongs to the $f\to fr$ transition are illustrated for the different lattice sizes at selected $D/J=-3$ and $K/J=-1$ where the $d\to f\to fr$ transition takes place. The behavior of the $g_L^{M_\alpha}$ for the $d\to f$ transition is similar with $g_L^{Q_d}$ for the $f\to fr$ transition and is not given here. It can be seen from Fig. 8(b) that the scaling data for the finite-size lattices lie on a single curve near the critical temperature when the value of the correlation length critical exponent is equal to the universal value of $\nu=0.64$. The data of the $g_L^{M_\alpha}$ and $g_L^{Q_d}$ are scaled with $\nu=0.64$ at selected D/J and K/J values.

Secondly, the critical temperatures are also obtained from the susceptibility maxima $T_c^{\chi_\alpha}(L)$ and $T_c^{\chi_d}(L)$. According to finite-size scaling theory, the infinite lattice critical temperature is given by

$$Tc(\infty)=Tc(L)+aL^{-1/\nu}. \tag{3.7}$$

Infinite lattice critical temperatures estimated from the extrapolation of susceptibilities peak temperatures to $1/L^{1/\nu}\to 0$ and from intersection of the Binder cumulant curves at finite lattices are given in Table 1.

Table 1: The estimated infinite lattice critical temperatures from the intersection of the Binder cumulants ($T_c^{g_L^{M_\alpha}}$ and $T_c^{g_L^{Qd}}$) and from the maxima of the susceptibilities ($T_c^{\chi_\alpha}$ and $T_c^{\chi_d}$).

D/J	K/J	$T_c^{g_L^{M_\alpha}}$	$T_c^{\chi_\alpha}$	$T_c^{g_L^{Qd}}$	$T_c^{\chi_d}$
		$d\to f$		$f\to fr$	
-8.9	-1	5.75±0.03	5.72±0.02	-	-
-3	-0.9	3.36±0.02	3.35±0.03	2.81±0.01	2.82±0.01
-3	-1	3.08±0.02	3.08±0.03	3.06±0.01	3.07±0.02
-3	-2.3	2.26±0.03	2.27±0.04	2.26±0.04	2.26±0.03
-3	-2.7	1.96±0.02	1.97±0.03	1.78±0.02	1.80±0.02
-3	-2.9	1.84±0.03	1.83±0.02	1.36±0.04	1.38±0.02
-3	-3	1.81±0.01	1.82±0.01	-	-
-1	-0.5	3.79±0.01	3.79±0.02	-	-
-1.5	-0.5	4.60±0.02	4.56±0.03	-	-
		$a\to fr$		$d\to a$	
-3	-1.3	2.87±0.01	2.87±0.04	3.42±0.01	3.39±0.03
-3	-1.5	2.79±0.04	2.81±0.02	3.41±0.04	3.42±0.03
-3	-2	2.54±0.01	2.56±0.03	2.90±0.02	2.88±0.03

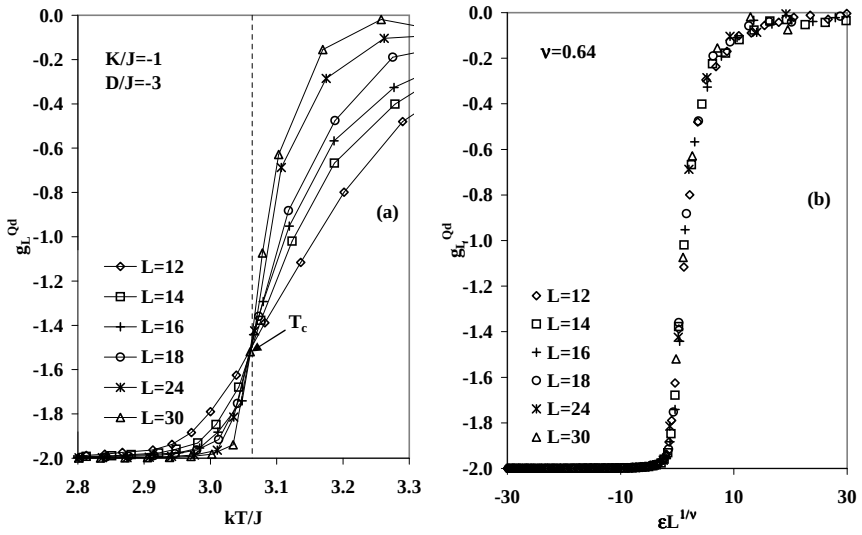

Figure 8: At $D/J=-3$ for $K/J=-1$ a) the Binder cumulant as a function of kT/J, b) finite size scaling plots of the Binder cumulant with $\nu=0.64$.

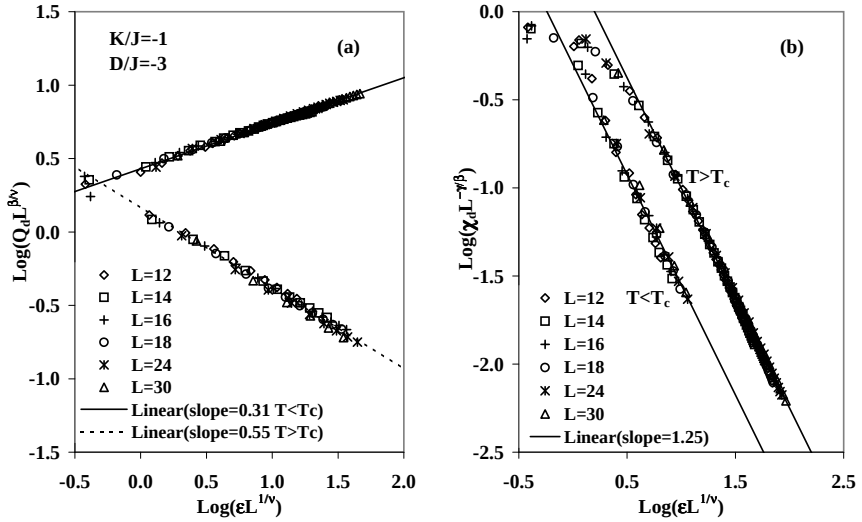

Figure 9: At $D/J=-3$ for $K/J=-1$ a) finite size scaling plots of order parameter Q_d, b) finite size scaling plots of the susceptibility χ_d, $\varepsilon=|T-T_c|/T_c$ for $T<T_c$ and $\varepsilon=|T-T_c|/T$ for $T>T_c$.

Moreover, the values of the static critical exponents β and γ are estimated using the FSS relations of the order parameters M_α and Q_d and susceptibilities χ_α and χ_d. The FSS relations for M and χ are given by

$$M=L^{-\beta/\nu}X(\varepsilon L^{1/\nu}), \tag{3.8}$$

$$kT\chi=L^{\gamma/\nu}Y(\varepsilon L^{1/\nu}). \tag{3.9}$$

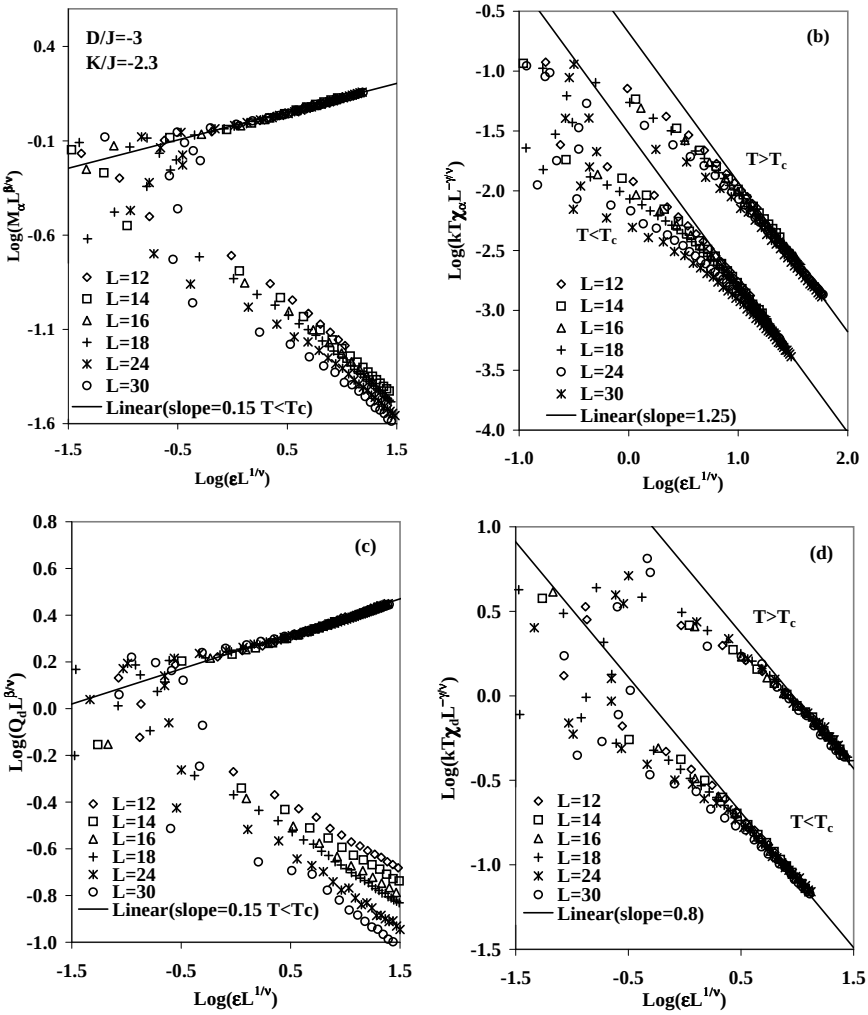

Figure 10: At $D/J=-3$ for $K/J=-2.3$ a) finite size scaling plots of order parameter M_α, b) finite size scaling plots of the susceptibility χ_α, $\varepsilon=|T-T_c|/T_c$ for $T<T_c$ and $\varepsilon=|T-T_c|/T$ for $T>T_c$, c) finite size scaling plots of order parameter Q_d, d) finite size scaling plots of the susceptibility χ_d, $\varepsilon=|T-T_c|/T_c$ for $T<T_c$ and $\varepsilon=|T-T_c|/T$ for $T>T_c$.

For large $x=\varepsilon L^{1/\nu}$, the infinite lattice critical behaviors must be asymptotically reproduced, that is,

$$X(x)=Ax^{\beta}, \tag{3.10}$$

$$Y(x)=Bx^{-\gamma}. \tag{3.11}$$

The finite-size scaling plots of the data for Q_d and χ_d according to the Eqs. (3.8) and (3.9) are shown in Fig. 9 for $D/J=-3$ and $K/J=-1$ parameter set. For $\beta=0.31$ and $\nu=0.64$ theoretical values, the data lie on a single curve for temperatures both below and

Table 2: The estimated β/ν and γ/ν values from finite-size scaling relations of the M_α, χ_α and Q_d, χ_d at $T_c(\infty)$.

		M_α, χ_α		Q_d, χ_d	
D/J	K/J	β/ν	γ/ν	β/ν	γ/ν
		$d \to f$		$f \to fr$	
-8.9	-1	0.49±0.03	1.93±0.04	-	-
-3	-0.9	0.45±0.03	1.91±0.02	0.49±0.02	1.88±0.04
-3	-1	0.48±0.02	1.91±0.03	0.47±0.04	1.95±0.01
-3	-2.3	0.23±0.02	1.69±0.03	0.25±0.02	1.22±0.05
-3	-2.7	0.48±0.02	1.92±0.03	0.49±0.03	1.93±0.02
-3	-2.9	0.50±0.03	1.97±0.02	0.47±0.03	1.68±0.02
-3	-3	0.49±0.02	1.96±0.03	-	-
-1	-0.5	0.49±0.02	1.94±0.04	-	-
-1.5	-0.5	0.47±0.02	1.97±0.03	-	-
		$a \to fr$		$d \to a$	
-3	-1.3	0.45±0.03	1.89±0.04	0.48±0.02	1.93±0.02
-3	-1.5	0.47±0.03	1.92±0.02	0.45±0.02	1.89±0.02
-3	-2	0.49±0.03	1.95±0.02	0.50±0.06	1.94±0.04

above $T_c(\infty)$ and are in agreement with the universal value of β=0.31 for $T<T_c(\infty)$. Also, the straight line passing through the data for $T>T_c(\infty)$ behaves according to Eq. (3.10) with $\beta'=0.55$ (Fig. 9(a)). Similarly, the scaling of χ_d data agrees with asymptotic form with the critical exponents $\gamma=\gamma'=1.25$ and $\nu=0.64$ for both $T<T_c(\infty)$ and $T>T_c(\infty)$ at selected parameters (Fig. 9(b)).

For all selected D/J and K/J values, the value of β and γ are in good agreement with theoretical ones except for $D/J=-3$ and $K/J=-2.3$ parameter set. For this parameter set, the scaling data of the order parameters M_α and the susceptibilities χ_α for the $a \to fr$ transitions, are shown in Fig. 10(a) and (b). It is obtained that the Binder cumulants $g_L^{M_\alpha}$ are scaled with the theoretical value $\nu=0.64$. But the order parameters M_α are not scaled with the $\beta=0.31$ and $\nu=0.64$, but scaled with $\beta=0.15$ and $\nu=0.64$ for the temperatures below $T_c(\infty)$ (Fig. 10(a)). On the other hand, the susceptibility (χ_α) data agree with the asymptotic form for the exponents $\gamma=\gamma'=1.25$ and $\nu=0.64$ for above and below $T_c(\infty)$. The scaling of the Q_d and χ_d are shown in Fig. 10(c) and (d) which belong the $d \to a$ transitions at the $D/J=-3$ and $K/J=-2.3$ parameter set. The Binder cumulant $g_L^{Q_d}$ is scaled with the theoretical value $\nu=0.64$, whereas the Q_d is scaled with $\beta=0.15$ and $\nu=0.64$ and χ_d data lie on a single curve for $\gamma=\gamma'=0.8$ and $\nu=0.64$ instead of the theoretical value $\gamma=\gamma'=1.25$.

Finally, we obtained the β/ν and γ/ν values from the finite-size scaling relations at $T_c(\infty)$. β/ν and γ/ν are estimated from the M_α and χ_α data for the $d \to f$ and $a \to fr$ transitions and from Q_d and χ_d for the $d \to a$ and $f \to fr$ transitions. The estimated values are given in Table 2. It is seen that the values of β and γ obtained from β/ν and γ/ν using $\nu=0.64$ are in agreement with ones obtained from the scaling.

4 Conclusion

In this paper, the spin-3/2 Ising model is simulated using the cooling algorithm of the cellular automaton on simple cubic lattice. The phase diagrams of the model are constructed in the (K/J, kT/J) plane for $D/J=0$ and -3 and in the (D/J, kT/J) plane for $K/J=-0.5$ and -1. It is shown that the d, f, fr and a phases occur in the phase diagrams and four different transitions such as $d\rightarrow f$, $d\rightarrow f\rightarrow fr$, $d\rightarrow f\rightarrow fr\rightarrow f$ and $d\rightarrow a\rightarrow fr$ take place for certain D/J and K/J values. According to our calculations, only $D/J=0$ phase diagram contains the re-entrant behavior at low temperatures. At $D/J=0$, the obtained phase diagram is in agreement with the results of MC simulation [3] and CVM [10] at the d-f and f-fr phase boundaries, but differs from MC and EFT [8] works in that the reentrant behavior does not occur at the f-fr phase boundary. The re-entrant behavior was also obtained within the MFA [3], CVM [12] predictions for $D/J=0$. The phase diagrams are also constructed in the (D/J, kT/J) plane for $K/J=-0.5$ and $K/J=-1$. Although the similar topologies are obtained for these parameters, the phase diagram for $K/J=-1$ has a multicritical point. On the other hand, multicritical points are also seen in the (K/J, kT/J) plane for $D/J=-3$. In addition, the temperature variations of the order parameters and associated susceptibilities are also studied. It is obtained that only the studying of the sublattice order parameters and susceptibilities do not suffice to consider the $d\rightarrow a$ transition whereas sublattice quantities can be considered for $d\rightarrow f$ and $f\rightarrow fr$ transitions. Therefore, the Q_d and χ_d quantities are also studied for all selected model parameters. In the second part of the study, the static critical exponents β and γ are estimated within the finite size scaling analysis. Except for $D/J=-3$ and $K/J=-2.3$, the model is compatible with universal Ising critical behavior ($\nu=0.64$, $\beta=0.31$ and $\gamma=\gamma'=1.25$) for all selected D/J and K/J parameter values. For this parameter set, the critical exponents are estimated from the sublattice quantities as $\nu=0.64$, $\beta=0.15$ and $\gamma=\gamma'=1.25$ and from Q_d ad χ_d as $\nu=0.64$, $\beta=0.15$ and $\gamma=\gamma'=0.8$.

Acknowledgments

This work was supported by the Scientific and Technological Research Council of Turkey (TÜBİTAK) Grant no: 109T018. We would also like to thank Turkish Republic General Directorate of Technical Research and Implementation(TAU)-Directorate of Computer of Center for some technical supports.

References

[1] J. Sivardiere and M. Blume, Dipolar and quadrupolar ordering in $S=3/2$ Ising systems, Phys. Rev. B 5 (1972), 1126-1134.

[2] S. Krinsky and D. Mukamel, Spin-3/2 Ising model for tricritical points in ternary fluid mixtures, Phys. Rev. B 11 (1975), 399-410.

[3] F.C. Sa Barreto and O.F. de Alcantara Bonfim, Phase transitions in the spin-3/2 BEG model, Physica A 172 (1991), 378-390.
[4] A. Bakchich, S. Bekhechi and A. Benyoussef, Multicritical behaviour of the antiferromagnetic spin-3/2 Blume-Capel model, Physica A 210 (1994), 415-423.
[5] A. Bakchich, A. Bassir and A. Benyoussef, Phase transitions in the spin-3/2 Blume-Emery-Griffiths model, Physica A 195 (1993), 188-196.
[6] A. Bakchich and M. El Bouziani, Position-space renormalization-group investigation of the spin-3/2 Blume-Emery-Griffiths model with repulsive biquadratic coupling, J. Phys. Condens. Matter 13 (2001), 91-99.
[7] T. Kaneyoshi and M. Jascur, Theory and phase diagram of a spin-3/2 BEG model, Phys. Lett. A 177 (1993), 172-176.
[8] A. Bakkali, M. Kerouad and M. Saber, The spin-3/2 Blume-Emery-Griffiths model, Physica A 229 (1996), 563-573.
[9] W. Jiang, G. Weib, A. Duc and L. Guoa, Phase diagrams and tricritical behavior in a spin-3/2 Ising model with transverse crystal field, Physica A 313 (2002), 503-512.
[10] J.W. Tucker, Cluster variational theory of spin-3/2 Ising models, J. Magn. Magn. Mater. 214, 121-129 (2000).
[11] M. Ali Pınar, M. Keskin, A. Erdinç, O. Canko, Critical behaviour of the ferromagnetic spin-3/2 Blume-Emery-Griffiths model with repulsive biquadratic coupling, Ze. Naturforsch. 62a (2007), 127-139.
[12] M. Keskin, O. Canko, Multicritical phase diagrams of the ferromagnetic spin-3/2 Blume-Emery-Griffiths model with repulsive biquadratic coupling including metastable phases: The cluster variation method and the path probability method with the point distribution, J. Magn. and Magn. Mater. 320 (2008), 8-24.
[13] S. Bekhechi and A. Benyoussef, Multicritical behavior of the antiferromagnetic spin-3/2 Blume-Capel model: Finite-size-scaling and Monte Carlo studies, Phys. Rev. B 56 (1997), 13954-13959.
[14] M. Creutz, Microcanonical Monte Carlo simulation, Phys. Rev. Lett. 50 (1983), 1411.
[15] B. Kutlu, The simulation of 2d ferromagnetic Blume–Capel model on a cellular automaton, Int. J. Mod. Phys. C 12 (2001), 1401-1413.
[16] B. Kutlu, A. Özkan, N. Seferoğlu, A. Solak and B. Binal, The Tricritical behavior of 3d Blume-Capel Model on a cellular automaton, Int. J. Mod. Phys. C 16 (2005), 933-950.
[17] N. Seferoğlu and B. Kutlu, Re-entrant phase transitions of the Blume–Emery–Griffiths model for a simple cubic lattice on the cellular automaton, Physica A 374 (2007), 165-172.
[18] N. Aktekin, Annual Reviews of Computational Physics VII, ed. D. Stauffer, pp.1-23 World Scientific, Singapore, 2000.
[19] B. Kutlu, The simulation of 2d spin-1 Ising model with positive biquadratic interaction on a cellular automaton, Int. J. Mod. Phys. C 14 (2003), 1305-1320.
[20] B. Kutlu, Critical behavior of the two-dimensional Ising model with next-nearest-neighbor antiferromagnetic interaction on the Creutz cellular automaton, Physica A 234 (1997), 807-818.
[21] N. Seferoğlu and B. Kutlu, Critical behavior of the Blume-Emery-Griffiths model for a simple cubic lattice on the cellular automaton, J. Stat. Phys. 129 (2007), 453-468.
[22] K. Binder, Z. Phys. B Condensed Matter 43 (1981), 119.
[23] V. Privman, Finite Size Scaling and Numerical Simulation of Statistical Systems, World Scientific, Singapore, 1990.